

## An IGWO-BP-based seeding depth detection system for no-till precision planters<sup>1</sup>

Desenvolvimento de um sistema de detecção da profundidade de semeadura em semeadoras de precisão para plantio direto baseado no algoritmo IGWO-BP

Hongqian Lv<sup>2</sup>, Jian Wang<sup>2</sup>, Xu Zhao<sup>2</sup>, Wenjun Wang<sup>2,3,4</sup>,  
Yulong Chen<sup>2,3,4</sup>, Long Zhou<sup>2,3,4</sup>, Mingwei Li<sup>2,3,4\*</sup> & Xiaomeng Xia<sup>2,3,4</sup>

<sup>1</sup> Research developed at Shandong University of Technology, Zibo, Shandong, China

<sup>2</sup> Shandong University of Technology/School of Agricultural Engineering and Food Science, Zibo, China

<sup>3</sup> Shandong University of Technology/Institute of Modern Agricultural Equipment, Zibo, China

<sup>4</sup> Shandong Provincial Key Laboratory of Smart Agricultural Technology and Intelligent Farm Machinery Equipment for Field Crops, Zibo, China

### HIGHLIGHTS:

An IGWO-BP model achieved  $R^2=0.91$  for seeding depth prediction, outperforming GWO-BP by 2.2% with 40% lower prediction error. Savitzky-Golay filtering reduced the force sensor noise by 26.4% SNRI compared to the particle filtering method. Field validation confirmed the accuracy of the model with  $R^2=0.90$ , MAE=0.03 cm, and RMSE=0.08 cm at multiple operating speeds.

**ABSTRACT:** Seeding depth is a key indicator for the evaluation of seeding quality, and has a significant impact on crop emergence and yield. However, accurate measurement of the seeding depth in a closed trench during the seeding process remains a challenge in the field of precision corn seeding. To solve these problems, this study presents a depth detection system based on IGWO-BP, in which a multi-sensor data fusion methodology is employed. Two filtering methods, particle filtering and Savitzky-Golay (SG) filtering, were compared for noise reduction in the force sensor data. The results show that SG filtering achieved the best noise reduction performance. The performance of seeding depth prediction models constructed based on the GWO-BP algorithm and the IGWO-BP algorithm was compared and analysed, and the results indicated that the IGWO-BP model achieved the best performance, with  $R^2 = 0.91$ , MAE = 0.03 cm, and RMSE = 0.08 cm. Further evaluation of the developed prediction model was conducted through field experiments, which revealed that IGWO-BP could accurately predict the seeding depth in closed trenches, with values of  $R^2 = 0.90$ , MAE = 0.03 cm, and RMSE = 0.08 cm. The proposed system integrated data from a speed sensor, force sensor, and inertial measurement units, and nine input parameters were considered in the prediction model. The dataset was divided into training and testing sets for model validation. The advances described in this study will be of great significance in improving the quality of precision seeding operations.

**Key words:** seeding depth detection, multi-sensor fusion, IGWO-BP algorithm, neural network optimisation

**RESUMO:** A profundidade de semeadura é um indicador fundamental para avaliar a qualidade da semeadura e tem um impacto significativo na emergência das plantas e na produtividade das culturas. No entanto, a medição precisa da profundidade de semeadura em sulcos fechados durante o processo de semeadura continua a ser um desafio no campo da semeadura de milho de precisão. Para resolver esse problema, este estudo desenvolveu um sistema de detecção de profundidade baseado em IGWO-BP, empregando uma metodologia de fusão de dados multissensoriais. Dois métodos de filtragem, Filtragem por Partículas e Filtragem Savitzky-Golay (SG), foram comparados para a redução de ruído nos dados do sensor de força. Os resultados demonstraram que a filtragem SG apresentou o melhor desempenho na redução de ruído. O desempenho dos modelos de predição da profundidade de semeadura, construídos com base nos algoritmos GWO-BP e IGWO-BP, foi comparado e analisado. Os resultados mostraram que o modelo IGWO-BP obteve o melhor desempenho, com  $R^2 = 0,91$ , MAE = 0,03 cm e RMSE = 0,08 cm. Uma avaliação adicional do modelo desenvolvido foi conduzida por meio de experimentos de campo. Os resultados indicaram que o IGWO-BP pôde prever com precisão a profundidade de semeadura em sulcos fechados, alcançando valores de  $R^2 = 0,90$ , MAE = 0,03 cm e RMSE = 0,08 cm. O sistema desenvolvido integra dados de um sensor de velocidade, sensor de força e unidades de medição inercial, considerando nove parâmetros de entrada no modelo de predição. O conjunto de dados foi dividido em conjuntos de treinamento e teste para validação do modelo. O progresso demonstrado neste estudo é de grande importância para melhorar a qualidade das operações de semeadura de precisão.

**Palavras-chave:** detecção da profundidade de semeadura, fusão multissensorial, algoritmo IGWO-BP, otimização de rede neural

**INTRODUCTION**

No-till fields have uneven surfaces, high soil firmness and the presence of plant residues, leading to poor consistency in the seeding depth. Studies have shown that this can reduce the corn yield by 314 kg hm<sup>-2</sup> (Yang et al., 2016; Poncet et al., 2018), meaning that the development of seeding depth detection technology is of great significance in terms of improving the informatisation of seeding quality and the intelligence of operations.

Previous studies have attempted to determine seeding depth through the use of ranging sensors or force sensors (Wen et al., 2014; Nielsen et al., 2016). However, in no-till conditions with straw residue and uneven soil surfaces, these methods are less appropriate, and have limited accuracy. Li et al. (2021) employed three flexible bending sensors (of a generic type rather than a brand name) to establish the relationship between the sensor signals and the downforce exerted by the gauge wheel, while Gao et al. (2020a) combined angle sensors with force sensors for depth estimation. Although these methods can provide a reference, they cannot accurately reflect the actual depths of seeds in closed trenches. Ground-penetrating radar has also been applied to this problem (Mapoka et al., 2019), but its high cost and sensitivity to soil water content and ion concentration limit its practical applicability.

Although the development of sensor technology now enables the real-time acquisition of multiple planter motion and force parameters (Xiao et al., 2015; Ji et al., 2016; Ma et al., 2023), converting this complex multi-sensor information into accurate seeding depth predictions remains challenging. Traditional linear models fail to capture the nonlinear coupling between soil conditions, machine dynamics, and downforce signals, and machine learning approaches such as

neural networks are therefore required. Backpropagation (BP) neural networks are well-suited to the modelling of nonlinear relationships, but easily become trapped in local minima due to their sensitivity to the initial weights and thresholds. The grey wolf optimisation (GWO) algorithm has been widely used to optimise neural networks, due to its simplicity and fast convergence, but it suffers from premature convergence. To overcome these shortcomings, this study introduces an improved grey wolf optimisation (IGWO) algorithm combined with a dynamic learning strategy to enhance the convergence speed, robustness, and generalisation of the BP neural network. (Xu et al., 2019; Zhang et al., 2022).

To address these limitations, this study aims to develop a multi-sensor fusion system for real-time seeding depth detection in closed trenches during no-till precision planting operations. The specific objectives are as follows: (i) to integrate multi-sensor data fusion for comprehensive capture of the planter dynamics; (ii) to develop an IGWO-BP algorithm for enhanced depth prediction accuracy; (iii) to optimise the processing of force sensor signals through noise reduction; and (iv) to validate the system performance under laboratory and field conditions. This research seeks to provide a cost-effective alternative to existing seeding depth detection methods while maintaining the accuracy required for precision agriculture applications.

**MATERIAL AND METHODS**

The proposed seeding depth detection system for a no-till precision planter comprises a speed measurement module, two inertial measurement units (IMUs) (Wit, Shenzhen, China, BWT61CL), a force sensor, and the no-till planter downforce prediction model, as shown in Figure 1. Speed measurements

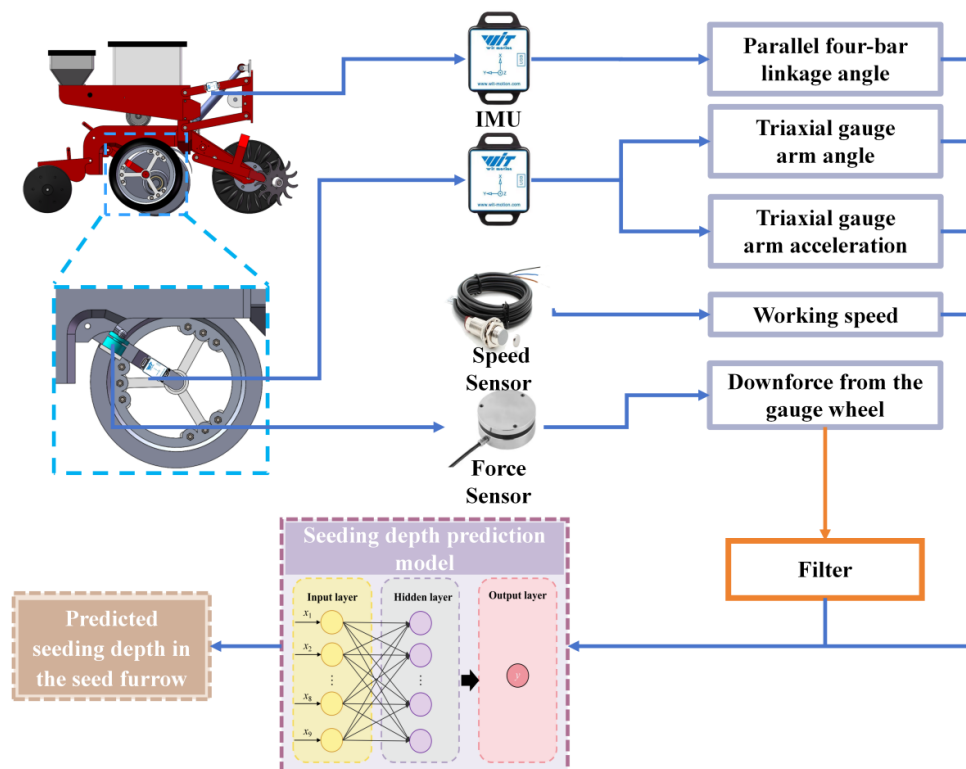


**Figure 1.** Proposed seeding depth detection system for a no-till precision planter

are used to detect the working speed of the planter in real time. IMUs are mounted on the parallel four-bar linkage and the gauge arm, and are used to collect data on the swing angle of the four-bar linkage and the three-axis angles and acceleration of the gauge arm. The force sensor, which is mounted on the inner side of the gauge arm, measures the force exerted on the arm. The operator changes the input current to the proportional relief valve (Beijing Huade, China, DBEM10-30B/200YM) by adjusting the input voltage to the proportional amplifier (Beijing Huade, China, VT-2000BS40), which in turn changes the output force on the hydraulic cylinder.

When the planter is in operation, the speed sensor collects information on the working speed of the planter, while the IMU measures the angles of the parallel four-bar linkage, the three-axis angles of the gauge arm and the acceleration, and the data are input into the seeding depth prediction model. The proposed depth prediction model based on a BP neural network outputs the predicted value of the seeding depth based on the working speed, four-link angle, gauge arm angle, acceleration, and the downward force exerted by the gauge wheel on the ground.

To obtain data for the construction of the seeding depth prediction model, experiments were conducted at the Modern Agricultural Equipment Laboratory of Shandong University of Technology (118° 00' 19.56" E, 36° 48' 18.18" N, elevation 53 m). The soil bin in the laboratory has dimensions of 60 × 3 × 0.8 m (length × width × depth). It contained brown soil consisting of loam, a common type of soil in cultivated land in North China. An electrically driven soil bin trolley was used to tow a no-tillage planter (Kangda, 2BMZF, China). This trolley provided a tractive force of 15 kN and a lifting force of 10 kN, with a total power output of 90 kW and a maximum speed of up to 10 km h<sup>-1</sup>. The no-till precision planter unit was a 2BMZF

model, and it was attached to the rear suspension of the soil bin trolley via a U-shaped clamp. A hydraulic cylinder was used to apply a downforce to the planter.

The experimental setup and data collection system are shown in Figure 2. The soil in the bin was treated based on the soil measurement results of the plough layer (0-10 cm). The soil was first rotary-tilled and irrigated, and after being allowed to dry naturally for some time, it was compacted using a roller. The processed soil had a moisture content of 15.38% ± 2% and a firmness of 2361 ± 100 kPa. The indoor experiment considered three factors: the working speed, the downward force exerted by the gauge wheel on the ground of the planter, and the terrain. The working speed was set to values of 3, 5, and 7 km h<sup>-1</sup>; the downward force exerted by the gauge wheel on the ground was set to 500, 1000 and 1500 N; and nine types of terrain were considered. The target seeding depth was 50 mm.

When the planter operates, the autocorrelation function of the planter's vibration characteristics could be distributed as a sine or cosine function. In this case, the undulation in the soil profile was constructed according to a sine function (Qing et al., 2021). The soil profile curve was calculated using Eq. 1:

$$y = A \sin\left(\frac{2\pi}{T} x\right) \tag{1}$$

where:

A - is the amplitude of the terrain relative to the reference plane, m; and,

T - is the wavelength of the terrain in the forward direction of the seeding machine, m.

During the experiment, the following parameters were recorded: the working speed, the swing angles of the parallel

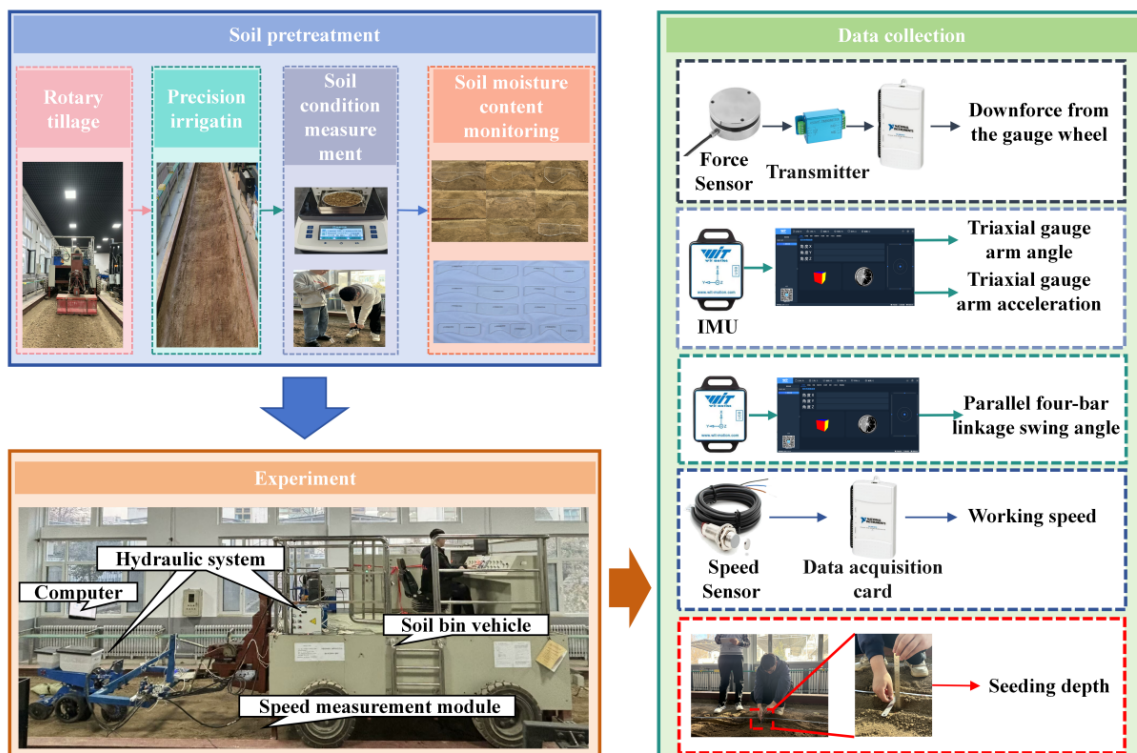


Figure 2. Experimental setup and data collection system

**Table 1.** Horizontal distribution of experimental factors

Level	Experimental factors	
	A (m)	T (m)
1	0.02	0.2
2	0.04	0.4
3	0.06	0.6

A - amplitude of the terrain relative to the reference plane; T - wavelength of the terrain in the forward direction of the seeding machine

four-bar linkage, the three-axis angles and accelerations of the gauge arm, the downward force exerted by the gauge wheel on the ground, and the actual seeding depth (Table 1). Both the IMU and the force sensor were sampled at 100 Hz and synchronised through the same data acquisition card to ensure time-aligned data streams with consistent timestamps.

To acquire the downward force exerted by the gauge wheel on the ground, a downforce measurement model based on the force sensor and IMU was established following the method of Gao et al. (2020b). An experimental bench was constructed for the indoor experiments, and a hydraulic cylinder was used to apply different levels of downward force to the planter. The output voltage of the force sensor was recorded with a data acquisition card (USB-6009, National Instruments, USA), and the rotation angle of the gauge arm was measured by the IMU. The actual downforce exerted by the gauge wheel was measured by an electronic scale placed beneath the planter. The relationship between the actual downforce exerted by the gauge wheel and the output signals of the force sensor and IMU was established based on the polynomial approximation fitting method, as shown in Eq. 2. A polynomial order was selected through cross-validation to avoid overfitting: higher-order polynomials were tested, but resulted in larger errors on validation data, and a lower-order polynomial was therefore adopted to ensure both accuracy and generalisation.

$$F = -7365.69 - 1225.47V + 253.31\alpha + 70.36V^2 - 2.18\alpha^2 + 19.66V\alpha \tag{2}$$

where:

F - is the downward force exerted by the gauge wheel on the ground, N;

V - is the output voltage of the force sensor, V; and,

α - is the rotation angle of the gauge arm, °.

A verification experiment was conducted to verify the accuracy of the downward force exerted by the gauge wheel on the ground. A similar method was implemented, except that the above growing gradually oil pressures were replaced with different values. The downforce was calculated based on the abovementioned relationship with the actual downforce measured by the electronic balance, and the mean absolute error (MAE) was used to evaluate the difference between the downforce calculated using the equation and the actual downforce measured by the electronic scale, as shown in Eq. 3.

$$MAE = \frac{1}{n} \sum_{i=1}^n |y_i - \hat{y}_i| \tag{3}$$

where:

y<sub>i</sub> - is the actual value, N; and,

ŷ<sub>i</sub> - is the predicted value, N.

As shown in Figure 3, the values predicted by the model lie close to the actual values, demonstrating good overall predictive performance. The MAE of the model is 27.8, indicating that the model has high accuracy and stability and can meet the measurement requirements for practical applications.

Sampling points were set at 25 cm intervals along the direction of the seeding rows after each experiment. The soil above the seeds was carefully removed until the seeds were exposed, and the vertical distance from the seed to the reference plane was measured as the actual seeding depth.

In this experiment, a speed measurement module based on a Hall sensor (CHE12-10NA-H710, HuChuang Industrial Co., Ltd., China) was used to determine the working speed of the planter. As shown in Figure 4, the guiding wheels of the soil bin trolley are equipped with four evenly distributed magnetic discs.

The Hall sensor generated a pulse signal when the magnetic disc rotating with the guide wheel passed through the sensor. The pulse signal intervals were recorded by the data acquisition card, and the speed was calculated as shown in Eq. 4:

$$v = 3.6 \times \frac{\pi r}{2t} \tag{4}$$

where:

v - is the working speed of the soil bin trolley, km h<sup>-1</sup>;

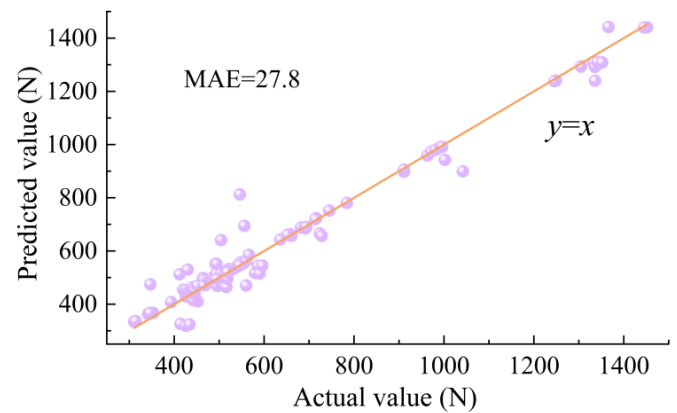


**Figure 3.** Results of the model verification experiment

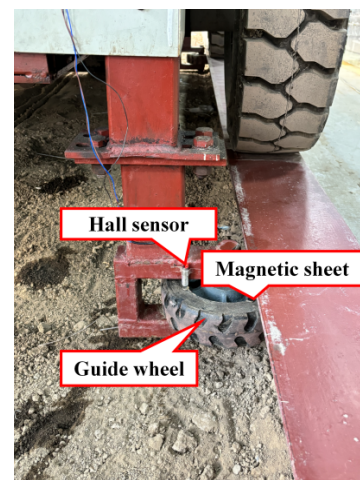


**Figure 4.** Photograph of the speed measurement module

$r$  - is the radius of the guiding wheel, 0.11 m; and,  
 $t$  - is the time measured by the Hall sensor in seconds, s.

The swing angle of the parallel four-bar linkage and the three-axis angle and acceleration of the gauge arm were collected using the IMU. The data were transmitted to the host computer via the Bluetooth module, and the host computer calculated the angle and acceleration data using the Kalman filter fusion algorithm. The resolution for the angular measurements was 0.0055°/LSB, the resolution of the acceleration measurements was 0.5 mg/LSB, the accuracy of the X and Y axes was 0.2°, and the accuracy of the Z axis was 1°. The raw IMU outputs of angles and accelerations were directly used as inputs to the neural network, without additional time-domain or frequency-domain feature extraction or normalisation.

The output signal of the force sensor is susceptible to environmental interference. The resulting noise may be erroneously interpreted as a valid feature by the BP neural network, thereby diminishing the model's generalisation capability. In this study, particle filtering (PF) (Wang & Ding, 2022) and SG filtering (Guo et al., 2023; Liu et al., 2024) were applied to preprocess the raw data from the force sensor.

PF is a nonlinear non-Gaussian state estimation method based on Bayesian estimation. It does not rely on the linearity of the system model or a Gaussian distribution of the noise, and has good flexibility and adaptability. PF achieves state estimation through three major steps: prediction, update and resampling.

The prediction phase can be expressed as shown in Eq. 5:

$$x_t^i = x_{t-1}^i + \eta_t^i, \eta_t^i \sim N(0, \sigma_p^2) \quad (5)$$

where:

$\sigma_p$  - is the standard deviation of the process noise, which is used to control the randomness of particle propagation, as shown in Eq. 6.

The update phase is expressed as:

$$w_t^i \propto w_{t-1}^i \times \exp\left[-\frac{(z_t - x_t^i)^2}{2\sigma_z^2}\right] \quad (6)$$

where:

$\sigma_z$  - is the standard deviation of the measurement noise, which reflects the confidence level of the observed data.

In this experiment, system resampling was triggered when the number of effective particles was less than half of the total number of particles, to ensure particle diversity and estimation accuracy.

The SG filtering algorithm is a data smoothing algorithm based on local polynomial fitting. SG filters are able to better preserve local features and details of the signal while effectively reducing noise interference. The mathematical essence of this process can be described as the optimal approximation of the signal using order- $n$  polynomials in a neighbourhood with a window width of  $2m+1$ . Assuming that the current time is  $t$ ,

with the data points within the window denoted as  $\{x_{t-m}, x_{t-m+1}, \dots, x_t, \dots, x_{t+m}\}$ , the fitted polynomial model is given by Eq. 7. In this study, the window is set to 15 and the polynomial order is set to third order.

$$x(t) \approx \sum_{i=0}^n a_i t^i, t \in [-m, m] \quad (7)$$

where:

$x(t)$  - is the signal value at relative position  $t$ ;  
 $a_i$  - is the coefficient of the fitted polynomial; and,  
 $n$  - is the order of the polynomial.

The performance of the two noise reduction algorithms was evaluated using MSEI (mean square error improvement) (Zhao et al., 2022), SNRI (signal-to-noise ratio improvement) (Li et al., 2008), RMSEI (root mean square error improvement) (Davis & Challis, 2020), and NCC (number of normalised correlations) (Li et al., 2008). In regard to error suppression, MSEI and RMSEI can be used to assess the accuracy by measuring the error in the signal before and after denoising, with larger values indicating better denoising performance. In regard to noise suppression, SNRI reflects the energy ratio between the signal and the noise, with higher values representing better noise reduction. In waveform correlation analysis, NCC is used to assess the structural similarity between the processed signal and the original signal; it takes values in the range  $[-1, 1]$ , where the closer the value is to one, the more completely the signal features are preserved. The evaluation metrics are calculated as shown in Eq. 8:

$$\left\{ \begin{array}{l} \text{MSEI} = \frac{|\text{MSE}_{\text{bf}} - \text{MSE}_{\text{af}}|}{\text{MSE}_{\text{bf}}}, \text{MSE} = \frac{1}{N} \sum_{i=1}^N (y_i - y)^2 \\ \text{SNRI} = \frac{|\text{SNR}_{\text{bf}} - \text{SNR}_{\text{af}}|}{\text{SNR}_{\text{bf}}}, \text{SNR} = 10 \log_{10} \left( \frac{P_{\text{signal}}}{P_{\text{noise}}} \right) \\ \text{RMSEI} = \frac{|\text{RMSE}_{\text{bf}} - \text{RMSE}_{\text{af}}|}{\text{RMSE}_{\text{bf}}}, \text{RMSE} = \sqrt{\frac{1}{N} \sum_{i=1}^N (y - y_i)^2} \\ \text{NCC} = \frac{\sum_{i=1}^n (x_i - \bar{x})(y_i - \bar{y})}{\sqrt{\sum_{i=1}^n (x_i - \bar{x})^2 \sum_{i=1}^n (y_i - \bar{y})^2}} \end{array} \right. \quad (8)$$

where:

$\text{MSE}_{\text{bf}}$  - is the MSE of the data before filtering;  
 $\text{MSE}_{\text{af}}$  - is the MSE of the data after filtering;  
 $N$  - is the number of data points;  
 $y_i$  - is the filtered data, V;  
 $y$  - is the true value, V;  
 $\text{SNR}_{\text{bf}}$  - is the SNR of the data before filtering;  
 $\text{SNR}_{\text{af}}$  - is the SNR of the data after filtering;  
 $P_{\text{signal}}$  - is the signal power;  
 $P_{\text{noise}}$  - is the noise power;  
 $\text{RMSE}_{\text{bf}}$  - is the RMSE of the data before filtering;  
 $\text{RMSE}_{\text{af}}$  - is the RMSE of the data after filtering;  
 $x_i$  - is the data before filtering, V;  
 $\bar{x}$  - is the mean value of the data before filtering, V;  
 $\bar{y}$  - is the mean value of the data after filtering, V; and,  
 $n$  - is the signal length.

The GWO algorithm uses the grey wolf position update mechanism to determine the optimal weights and thresholds for the BP neural network. The GWO optimisation search process can be divided into three phases: encirclement, pursuit and attack. In the encirclement phase, the grey wolf first approaches the optimal position by continuously adjusting its position, thus providing a better starting point for the chase and attack phases. In this process, the top three best performing individuals in the population are referred to as  $\alpha$ ,  $\beta$ , and  $\delta$  wolves, representing the leader and the two co-leaders, respectively. Their positions are used to guide the direction of the position updates of the remaining individuals, thus enhancing the population's ability to steer in the search space with the speed of convergence. The  $\alpha$  wolf usually represents the currently found optimal solution, while the  $\beta$  and  $\delta$  wolves provide sub-optimal references; together, these are used to construct a direction vector approaching the optimal solution, thus achieving effective guidance of the search process. The position updating formula is given in Eqs. 9 to 13 below.

$$\begin{cases} D_\alpha = |C_1 \times X_\alpha - X_i| \\ D_\beta = |C_2 \times X_\beta - X_i| \\ D_\delta = |C_3 \times X_\delta - X_i| \end{cases} \quad (9)$$

$$\begin{cases} X_1 = X_\alpha - A_1 D_\alpha \\ X_2 = X_\beta - A_2 D_\beta \\ X_3 = X_\delta - A_3 D_\delta \end{cases} \quad (10)$$

$$A = 2ar_1 - a \quad (11)$$

$$C = 2r_2 \quad (12)$$

$$a = 2 - \frac{2t}{T} \quad (13)$$

where:

$D_\alpha$ ,  $D_\beta$  and  $D_\delta$  - are the distances between the  $\alpha$ ,  $\beta$  and  $\delta$  wolves and the other individuals, respectively;

$A$  and  $C$  - are the coefficient vectors;

$X_\alpha$ ,  $X_\beta$  and  $X_\delta$  - are the current positions of the  $\alpha$ ,  $\beta$  and  $\delta$  wolves, respectively;

$a$  - is a control factor;

$r_1$  and  $r_2$  - are random vectors in the range  $[0,1]$ ;

$t$  - is the current iteration count; and,

$T$  - is the maximum number of iterations.

Dynamic learning strategy (DLH) is an optimisation strategy based on neighbourhood intelligence with adaptive search and enhanced diversity (Nadimi-Shahraki et al., 2021; Chen et al., 2025). In this study, an improved optimisation algorithm was constructed by integrating the neighbourhood learning mechanism of DLH with the hierarchical search structure of GWO. More specifically, while maintaining the  $\alpha$ ,  $\beta$  and  $\delta$  leadership levels in GWO, the algorithm combines

the dynamic neighbourhood search mechanism of DLH with the candidate position calculation of GWO to form a dual position updating strategy. This fusion mechanism not only maintains the hierarchical search feature of GWO, but also enhances the local development ability and population diversity of the algorithm by using the neighbourhood learning process of DLH. The expression for the position update of DLH in IGWO is shown in Eq. 14.

$$X_{t,d}^{DLH} = X_{t,d} + r \times (X_{n_{a,d}} - X_{r,d}) \quad (14)$$

where:

$X_{t,d}^{DLH}$  - is the updated DLH position of the  $t$ -th individual in the  $d$ -th dimension;

$X_{t,d}$  - is the position of the  $t$ -th individual in the  $d$ -th dimension in the original population;

$X_{n_{a,d}}$  - is the position of the  $d$ -th dimensional random neighbour of the  $t$ -th individual;

$X_{r,d}$  - is the position of an individual randomly selected from the whole population in the  $d$ -th dimension; and,

$r \sim U(0,1)$  - is a random number that follows a uniform distribution.

In the DLH strategy, the neighbourhood of an individual is defined dynamically, by selecting one random neighbour from the population and one additional random individual from the entire population. These two references jointly define the candidate update direction. Only candidates that improve the individual's fitness are retained, thus serving as an implicit screening mechanism. This design ensures diversity while preventing poor-quality neighbours from misleading the search.

In the IGWO algorithm, the neighbourhood of an individual is also defined dynamically. In this case, each individual selects one random neighbour from the local population and one additional random individual from the entire population. These two references jointly define the neighbourhood and guide the position update. This strategy strikes a balance between local and global exploration. Furthermore, the fitness evaluation acts as an implicit screening mechanism, ensuring that updates from poor-quality neighbours are not retained. Combined with the  $\alpha$ ,  $\beta$ , and  $\delta$  leadership structure of GWO, this design prevents premature convergence and enhances the robustness of the search.

In terms of BP neural network optimisation, IGWO involves a new search mechanism that combines the advantages of the two algorithms. The proposed hybrid algorithm preserves the hierarchical structure of GWO, characterised by the  $\alpha$ ,  $\beta$  and  $\delta$  leadership levels, while incorporating the dynamic neighbourhood search strategy of DLH into GWO's candidate position update process to form a cooperative optimisation framework. This algorithm not only maintains the hierarchical search feature of GWO, but also enhances the accuracy and diversity of position adjustment through the neighbourhood learning mechanism of DLH, thereby finding the optimal parameter combination in the solution space more effectively. The details of the optimisation process in IGWO-BP is illustrated in the flowchart in Figure 5.

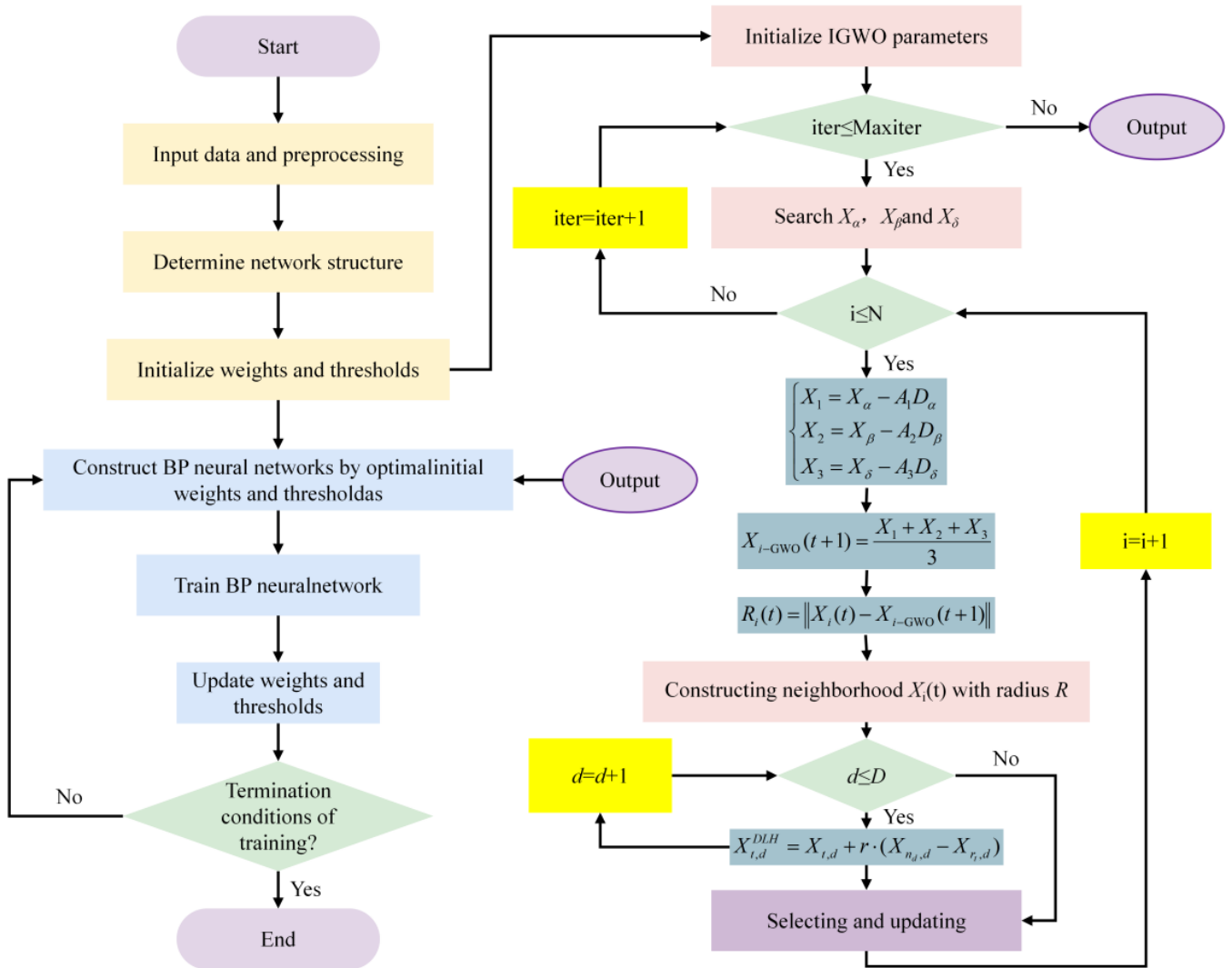


Figure 5. Flowchart for IGWO-BP

When training IGWO-BP, the dataset was divided into a training set and test set at a ratio of 70:30 to evaluate the generalisation degree of the model. The BP neural network considered in this study consisted of one hidden layer with 12 nodes, in which a sigmoid activation function was adopted in the hidden layer and the output layer used a linear activation function. The model was trained with a learning rate of 0.01 for 1000 iterations, and all input variables were normalised before training.

To evaluate the performance and reliability of the seeding depth prediction model, the coefficient of determination ( $R^2$ ) (Sun & Huang, 2020; Huang et al., 2022), the mean absolute error (MAE) (Huang et al., 2022) and the root mean square error (RMSE) (Sun & Huang, 2020; Huang et al., 2022) were used as evaluation indices of the model's predictive performance, as shown in Eq. 15.  $R^2$  was used to assess the model's ability to explain the variability in the data, where values closer to one indicate a better fit to the data distribution. MAE directly reflects the accuracy of the model's predictions by calculating the mean absolute deviation of the predicted value from the true value, with smaller values indicating better performance. Compared with MAE, RMSE has an increased sensitivity to larger errors, with smaller values representing better predictive stability of the model.

$$\left\{ \begin{array}{l} R^2 = 1 - \frac{\sum_{i=1}^N (y_i - \hat{y}_i)^2}{\sum_{i=1}^N (y_i - \bar{y})^2} \\ MAE = \frac{1}{N} \sum_{i=1}^N |y_i - \hat{y}_i| \\ RMSE = \sqrt{\frac{1}{N} \sum_{i=1}^N (y_i - \hat{y}_i)^2} \end{array} \right. \quad (15)$$

where:

- N - is the number of samples;
- $y_i$  - is the actual value, cm;
- $\hat{y}_i$  - is the predicted value, cm;
- $\bar{y}$  - is the mean of the actual values, cm; and,
- n - is the number of samples.

A field experiment was conducted in Linzi District, Zibo City (118° 29' 30" E, 37° 00' 30" N) in December 2024 to explore the applicability of the proposed seeding depth prediction model. Before the experiment, the soil moisture content was measured as  $18 \pm 2\%$ , and the soil firmness was  $2700 \pm 300$  kPa.

The target downforce of the planter against the ground was set to 1000 N, and the working speeds were set to 3, 5 and 7 km h<sup>-1</sup>, respectively. During the experiment, the working speed of the planter, the swing angles of the parallel four-bar linkage, the three-axis angle and acceleration of the gauge arm, and the downward force exerted by the gauge wheel on the ground were collected in real time. After the experiment, the actual operational values of the seeding depth were collected at intervals of 25 cm along the seeding row. After seeding, the soil was excavated to expose each seed, and the vertical distance from the seed to the soil surface was measured directly. The predictive performance of the model was evaluated using the R<sup>2</sup>, MAE, and RMSE as evaluation indices. The experimental site and sampling method are shown in Figure 6.

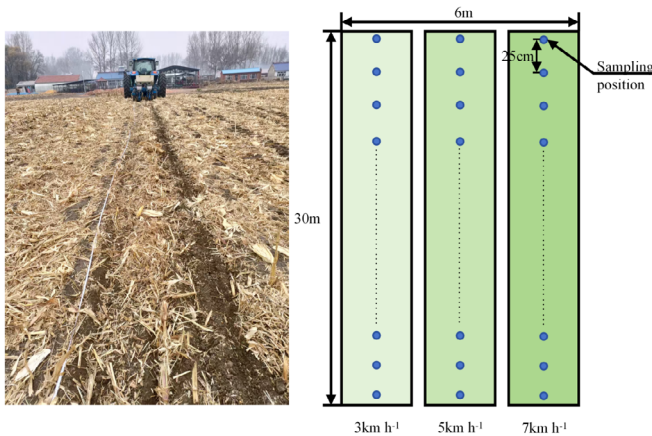


Figure 6. Experimental site and sampling method

### RESULTS AND DISCUSSION

Noise reduction processing of the force sensor data was carried out with two filtering algorithms, namely PF and SG, and the results are shown in Figure 7. The performance of the two algorithms was quantified using MSEI, SNRI, RMSEI, and NCC (Figure 8). Compared with PF, SG filtering improved MSEI by 5.4%, SNRI by 26.4%, and RMSEI by 8.5%, while maintaining an NCC of 0.93. These results indicate that SG filtering more effectively reduces noise while preserving the main waveform features. From an agricultural perspective, this means cleaner input data for the prediction model, thereby improving the reliability of seeding depth estimation. Although

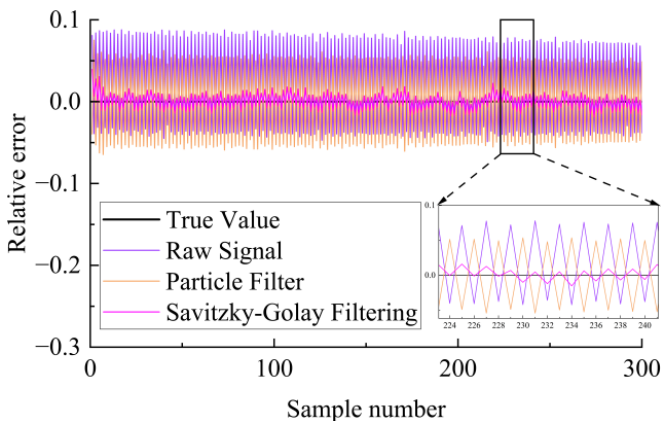


Figure 7. Comparison of relative errors after noise reduction of force sensor data

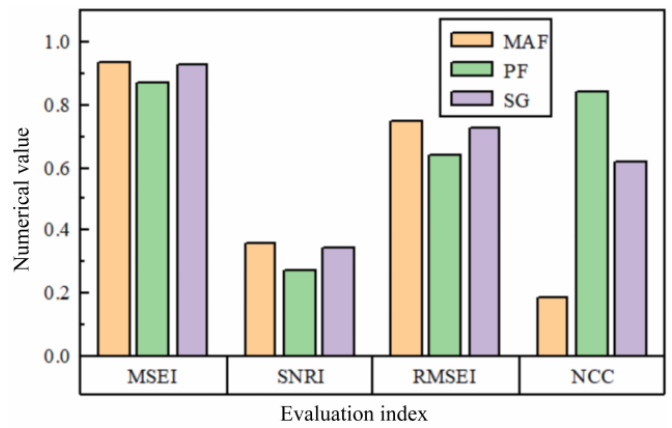


Figure 8. Performance of different noise reduction algorithms

PF achieved slightly higher waveform correlation, it is computationally more demanding and may introduce spurious noise, making it less suitable for real-time planter applications. In contrast, SG filtering requires fewer computational resources and is easier to implement on embedded hardware, which is essential for real-time seeding operations. Hence, SG was selected as the denoising algorithm in this study.

Figure 9 shows the prediction results for the seeding depth obtained with the GWO-BP and IGWO-BP models on the training set, with the data points representing the relative errors between the model predictions and actual values. Compared with the GWO-BP model, the predictions of the IGWO-BP model show less fluctuation, which indicates that the seeding depth predicted by the IGWO-BP model is closer to the true value. The predictive performance of the two predictive models on the training set is shown in Figure 9. IGWO-BP achieved a 2.2% increase in R<sup>2</sup>, a 40% reduction in MAE, and a 27.3% reduction in RMSE relative to GWO-BP, clearly demonstrating higher accuracy and stability.

Compared to GWO-BP, IGWO-BP had an R<sup>2</sup> that was improved by 2.2%, with reductions in MAE and RMSE of 40.0 and 27.3%, respectively. These results demonstrate that IGWO-BP provides a more accurate fit to the actual values, with fewer large deviations. More importantly, the improvements have direct agricultural implications: more stable seeding depth predictions contribute to a more uniform seed placement, which is essential for consistent crop emergence and yield. From a practical perspective, IGWO-BP requires more computational iterations than standard GWO-BP, but the additional cost is justified by the gains in accuracy. Modern embedded processors can accommodate these computations, although parameter tuning and a longer runtime must be considered for real-time field deployment. Hence, the IGWO-BP model yields superior predictive performance in terms of seeding depth.

As shown in Figure 10, the value of R<sup>2</sup> for both the GWO-BP and IGWO-BP models remained at or above 0.89 on the experimental set. These results show that the models' performance on the experimental set is consistent with that on the training set, without significant overfitting. IGWO-BP outperformed GWO-BP in terms of all evaluation indices. Compared with GWO-BP, the R<sup>2</sup> for IGWO-BP was increased by 2.2%, the MAE was reduced by 50%, and the RMSE decreased by 33.3%. These results indicate that IGWO-BP has a definite advantage in predicting seeding depth.

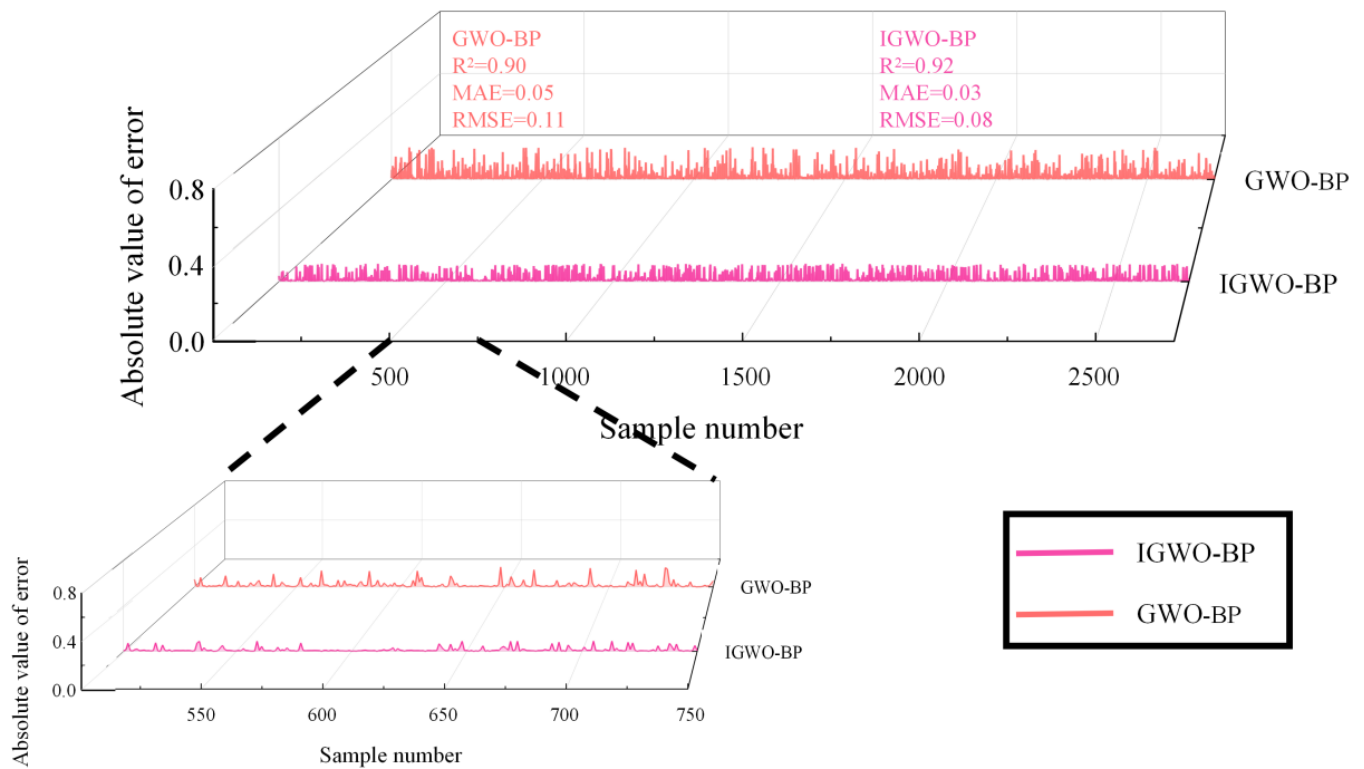


Figure 9. Model prediction results for the training set

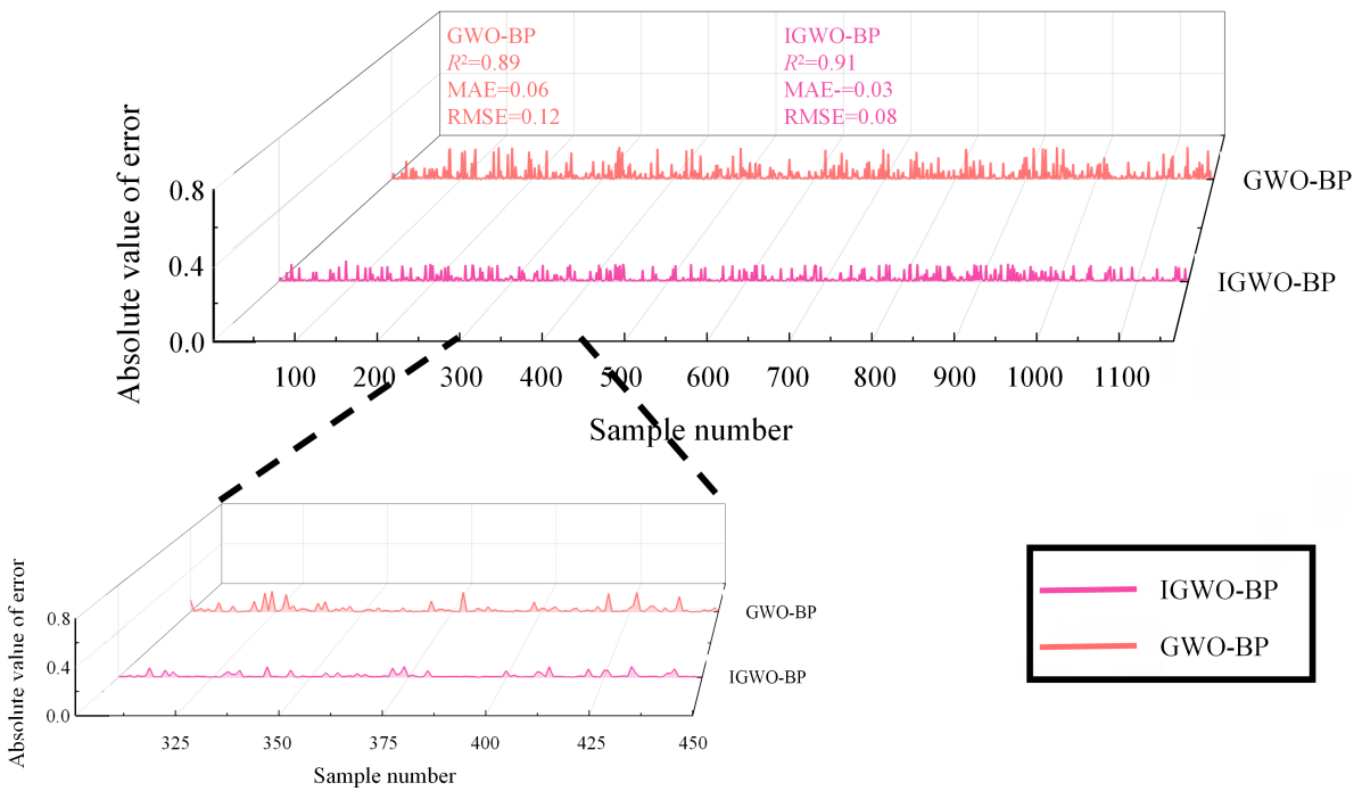
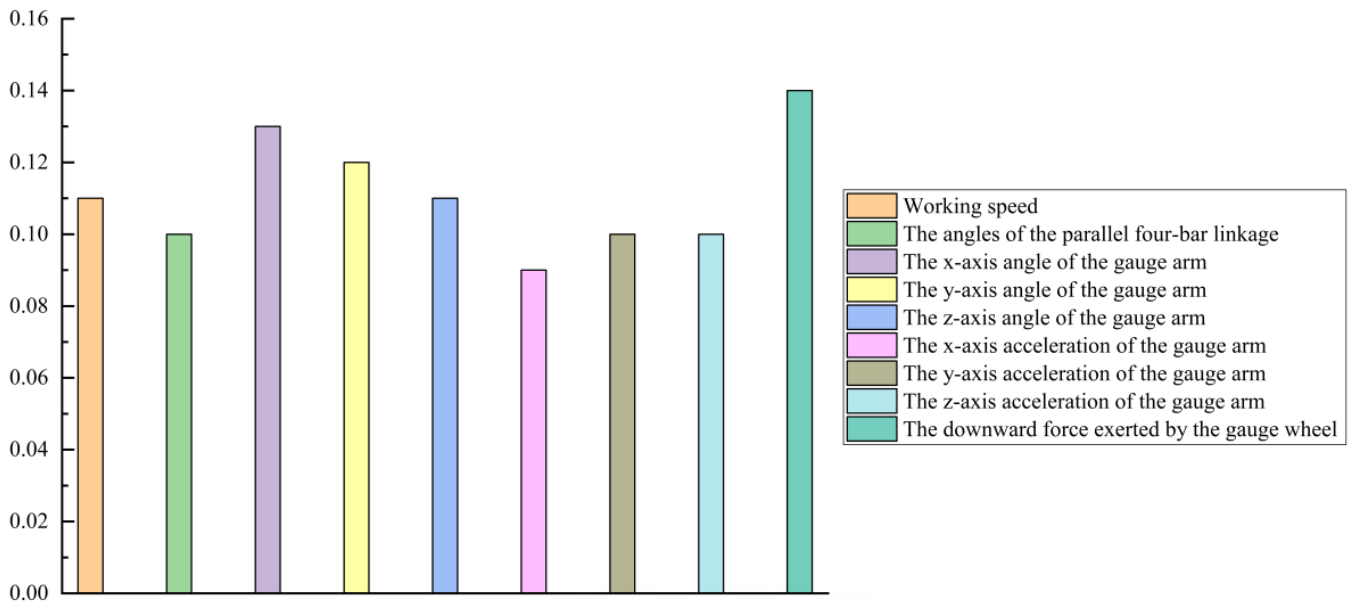


Figure 10. Model prediction results for the experimental set

To further evaluate the sensitivity of the seeding depth prediction to differences in the input variables, we calculated the relative contribution of each feature using the Garson algorithm, based on the trained IGWO-BP neural network. The results are shown in Figure 11.

Each of the nine input variables, including the working speed, the angle of the parallel four-bar linkage, the three-axis

angles and accelerations of the gauge arm, and the downward force exerted by the gauge wheel, contributed approximately 9-15% to the prediction results. This range is close to the theoretical equal share of 11.1%, indicating that all input variables play a role in prediction and no single feature dominates the output. This analysis provides clear evidence that the proposed multi-sensor fusion framework achieves



**Figure 11.** Relative contributions of the nine input variables to seeding depth predictions in the IGWO-BP model

balanced utilisation of the collected information, and confirms the sensitivity of the seeding depth to each variable.

The prediction results for seeding depth were obtained by inputting the multi-sensor data collected from the applicability experiment into the established IGWO-BP neural network model. A comparison between the predicted values obtained from the model and the measured values is shown in Figure 12.

The  $R^2$  for the model is 0.90, the MAE is 0.03, and the RMSE is 0.08. These results are close to the laboratory values ( $R^2 = 0.91$ , MAE = 0.03, RMSE = 0.08), and the small differences can be explained by the firmness of the soil ( $2361 \pm 100$  kPa in lab vs.  $2700 \pm 300$  kPa in field), the soil moisture ( $15.4 \pm 2\%$  vs.  $18 \pm 2\%$ ), and additional field disturbances such as vibration and operator variability. These factors demonstrate that even modest changes in soil and operating conditions can influence the prediction accuracy. The research results show that the constructed prediction model can effectively fit the relationship between the output information of the sensor and the seeding depth of the planter.

Nevertheless, several practical limitations of this research should be acknowledged. Firstly, sensors require periodic calibration, and force sensors in particular may drift under prolonged field use. Secondly, validation was performed on

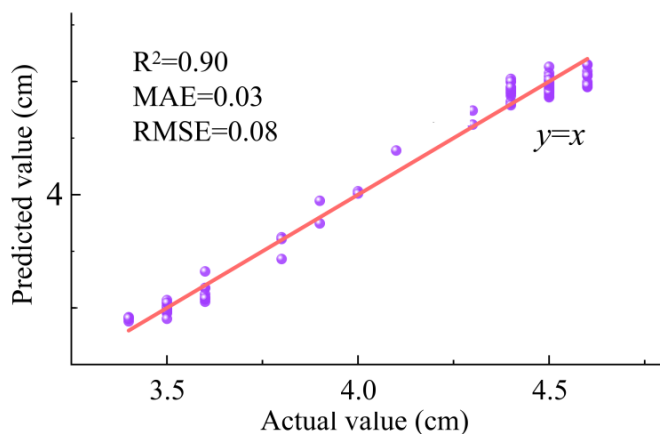


**Figure 12.** Relationship between predicted and actual values of seeding depth

loam soil, and further testing on sandy and clay soils will be needed to assess the generalisability of this approach. Thirdly, operator training and correct installation are necessary, as improper handling of the sensors can reduce the performance. Addressing these limitations will be critical to ensure the robustness and feasibility of adoption of the proposed system in diverse agricultural environments.

### CONCLUSIONS

1. Multi-sensor fusion successfully enabled real-time seeding depth detection in closed trenches, addressing a critical gap in no-till precision agriculture.
2. The integrated system combined speed sensors with inertial measurement units and force sensors, thereby capturing the comprehensive dynamics of the planter, which the individual sensors could not achieve alone.
3. The IGWO-BP algorithm demonstrated superior prediction accuracy compared to conventional approaches, with field validation confirming practical applicability across varying operational conditions.
4. SG filtering proved most effective for agricultural sensor signal processing, and significantly improved the reliability of measurement under field conditions.
5. Validation based on a range of soil types and an economic feasibility analysis will be necessary for widespread commercial implementation.

**Contribution of authors:** Hongqian Lv: participation in the design of the research, collection, analysis and interpretation of data, preparation of the manuscript, drafted the manuscript, literature review. Jian Wang: collection, analysis and interpretation of data. Xu Zhao: collection, analysis and interpretation of data. Wenjun Wang: administration and acquisition of financing, supervision of the work, preparation of the manuscript. Yulong Chen: supervision of the work. Long Zhou: administration and acquisition of financing, supervision of the work. Mingwei Li: administration and

acquisition of financing, supervision of the work. Xiaomeng Xia: participation in the design of the research, preparation of the manuscript, literature review, supervision of the work, drafted the manuscript.

**Data availability statement:** The raw/processed data required to reproduce these findings cannot be shared at this time as the data also forms part of an ongoing study.

**Conflict of interest:** The authors declare no conflict of interest.

**Financing statement:** There was no source of funding for the research.

**Acknowledgement:** This work was supported by the National Key Research and Development Program of China (2024YFD2000404-03), Natural Science Foundation of China (52405280), Natural Science Foundation of Shandong Province (ZR2024QE004, ZR2023QF143, ZR2023QE198), High-quality Development Project for the Ministry of Industry and Information (2023ZY02009), Youth Innovation Team Development Plan for Higher Education Institutions in Shandong Province (2022KJ225).

## LITERATURE CITED

- Chen, H. F.; Yu, P.; Long, J. Q. Multi-objective optimization of automotive seat frames using machine learning. *Advances in Engineering Software*, v.199, e103797, 2025. <https://doi.org/10.1016/j.advengsoft.2024.103797>
- Davis, D. J.; Challis, J. H. Automatic segment filtering procedure for processing non-stationary signals. *Journal of Biomechanics*, v.101, e109619, 2020. <https://doi.org/10.1016/j.jbiomech.2020.109619>
- Gao, Y. Y.; Zhai, C. Y.; Yang, S.; Zhao, X. G.; Wang, X.; Zhao, C. J. Development of CAN-based downforce and sowing depth monitoring and evaluation system for precision planter. *Transactions of the Chinese Society of Agricultural Machinery*, v.51, p.15-28, 2020a. <https://doi.org/10.6041/j.issn.1000-1298.2020.06.002>
- Gao, Y. Y.; Zhai, C. Y.; Yang, S.; Zhao, X. G.; Wang, X.; Zhao, C. J. Measurement method and mathematical model for the seeding downforce of planter row unit. *Transactions of the Chinese Society of Agricultural Engineering*, v.36, p.1-9, 2020b. <https://doi.org/10.11975/j.issn.1002-6819.2020.05.001>
- Guo, F.; Wu, X. W.; Liu, L. L.; Ye, J. L.; Wang, T.; Fu, L. J.; Wu, Y. P. Prediction of remaining useful life and state of health of lithium batteries based on time series feature and Savitzky-Golay filter combined with gated recurrent unit neural network. *Energy*, v.270, e126880, 2023. <https://doi.org/10.1016/j.energy.2023.126880>
- Huang, X. Q.; Li, Q.; Tai, Y. H.; Chen, Z. Q.; Liu, J.; Shi, J. S.; Liu, W. M. Time series forecasting for hourly photovoltaic power using conditional generative adversarial network and Bi-LSTM. *Energy*, v.246, e123403, 2022. <https://doi.org/10.1016/j.energy.2022.123403>
- Ji, Y. H.; Jiang, Y. Q.; Li, T.; Zhang, M.; Sha, Sha.; Li, M. Z. An improved method of tomato photosynthetic rate prediction based on WSN in greenhouse. *International Journal of Agricultural and Biological Engineering*, v.9, p.146-152, 2016. <https://doi.org/10.3965/j.ijabe.20160901.1243>
- Li, M. W.; Xia, X. M.; Zhu, L. T.; Zhou, R. Y.; Huang, D.Y. Intelligent sowing depth regulation system based on Flex sensor and Mamdani fuzzy model for a no-till planter. *International Journal of Agricultural and Biological Engineering*, v.14, p.145-152, 2021. <https://doi.org/10.25165/j.ijabe.20211406.5939>
- Li, P.; Tang, J.; Zhang, X. X. An algorithm of complex self-adaptive block threshold for extracting PD signal. *Transactions of China Electrotechnical Society*, v.23, p.112-117, 2008. <https://doi.org/10.19595/j.cnki.1000-6753.tces.2008.07.019>
- Liu, S. J.; Xu, T.; Du, X. Z.; Zhang, Y. C.; Wu, J. B. A hybrid deep learning model based on parallel architecture TCN-LSTM with Savitzky-Golay filter for wind power prediction. *Energy Conversion and Management*, v.302, e118122, 2024. <https://doi.org/10.1016/j.enconman.2024.118122>
- Mapoka, K.; Birrell, S. J.; Tekeste, M. A comprehensive survey of nondestructive sensing technologies for the detection of corn seeds in a closed trench and measuring planting depth to augment the conventional method. *Computers and Electronics in Agriculture*, v.158, p.249-257, 2019. <https://doi.org/10.1016/j.compag.2019.02.010>
- Ma, Z.; Zhu, Y. L.; Wu, Z. P.; Traore, S. N.; Chen, D.; Xing, L. C. BP neural network model for material distribution prediction based on variable amplitude anti-blocking screening DEM simulations. *International Journal of Agricultural and Biological Engineering*, v.16, p.190-199, 2023. <https://doi.org/10.25165/j.ijabe.20231604.7178>
- Nadimi-Shahraki, M. H.; Taghian, S.; Mirjalili, S. An improved grey wolf optimizer for solving engineering problems. *Expert Systems with Applications*, v.166, e113917, 2021. <https://doi.org/10.1016/j.eswa.2020.113917>
- Nielsen, S. K.; Nørremark, M.; Green, O. Sensor and control for consistent seed drill coulter depth. *Computers and Electronics in Agriculture*, v.127, p.690-698, 2016. <https://doi.org/10.1016/j.compag.2016.07.029>
- Poncet, A. M.; Fulton, J. P.; McDonald, T. P.; Knappenberger, T.; Shaw, J. N.; Bridges, R. W. Effect of heterogeneous field conditions on corn seeding depth accuracy and uniformity. *Applied Engineering in Agriculture*, v.34, p.819-830, 2018. <https://doi.org/10.13031/aea.12238>
- Sun, W.; Huang, C. C. A carbon price prediction model based on secondary decomposition algorithm and optimized back propagation neural network. *Journal of Cleaner Production*, v.243, e118671, 2020. <https://doi.org/10.1016/j.jclepro.2019.118671>
- Tang, Q.; Wu, J.; Jiang, L.; Wu, C. Y.; Xiao, T. Q.; Jiang, T. Design and Test of Hydraulic Profiling System for Rape Seedling Combined Transplanter. *Transactions of the Chinese Society of Agricultural Machinery*, v.52, e1213, 2021. <https://doi.org/10.6041/j.issn.1000-1298.2021.11.010>
- Wang, X. H.; Ding, F. Modified particle filtering-based robust estimation for a networked control system corrupted by impulsive noise. *International Journal of Robust and Nonlinear Control*, v.32, p.830-850, 2022. <https://doi.org/10.1002/rnc.5850>
- Wen, L. P.; Fan, X. F.; Liu, Z.; Zhang, Y. The design and development of the precision planter sowing depth control system. *Sensors & Transducers*, v.162, p.53, 2014.
- Xiao, C. Y.; Zheng, L. H.; Li, M. Z.; Chen, Y.; Mai, C. Y. Apple detection from apple tree image based on BP neural network and Hough transform. *International Journal of Agricultural and Biological Engineering*, v.8, p.46-53, 2015. <https://doi.org/10.3965/j.ijabe.20150806.1239>

- Xu, L. W.; Wang, H.; Lin, W.; Gulliver, T. A.; Le, K. N. GWO-BP neural network based OP performance prediction for mobile multiuser communication networks. *IEEE Access*, v.7, p.152690-152700, 2019. <https://doi.org/10.1109/ACCESS.2019.2948475>
- Yang, L.; Yan, B. X.; Zhang, D. X.; Zhang, T. L.; Wang, Y. X.; Cui, T. Research progress on precision planting technology of maize. *Transactions of the Chinese Society of Agricultural Machinery*, v.47, e4545, 2016. <https://doi.org/10.6041/j.issn.1000-1298.2016.11.006>
- Zhang, X.; Hou, J. W.; Wang, Z. K.; Jiang, Y. Q. Joint SOH-SOC estimation model for lithium-ion batteries based on GWO-BP neural network. *Energies*, v.16, e132, 2022. <https://doi.org/10.3390/en16010132>
- Zhao, N. C.; Zhao, B.; Yi, S. J.; Zhou, Z.; Che, G. Research on a sowing depth detection system based on an improved adaptive kalman filtering method. *Electronics*, v.11, e3802, 2022. <https://doi.org/10.3390/electronics11223802>